Article:
Slatter, T., Zalzalah, M. and Lewis, R. (2023) Analysis of reciprocating hammer type impact wear apparatus. Wear, 523. 204816. ISSN: 0043-1648

https://doi.org/10.1016/j.wear.2023.204816

Wear 523 (2023) 204816

Contents lists available at ScienceDirect

Wear

journal homepage: www.elsevier.com/locate/wear

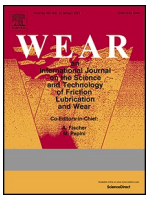

Analysis of reciprocating hammer type impact wear apparatus

Tom Slatter *, Mohanad Zalzalah, Roger Lewis

Department of Mechanical Engineering, The University of Sheffield, Mappin Street, Sheffield, S1 3JD, UK

ARTICLE INFO

Keywords:
Impact wear
Wear testing
Reciprocating hammer
Percussive wear

ABSTRACT

Repetitive impact wear of metals is caused by primary wear mechanisms removing material from the surfaces and is responsible either solely, or in part, for the failure of engineering components (e.g. automotive valvetrains, wheel-rail contacts, mining equipment). Fundamental work exists, but overwhelmingly considers the impact wear of a particular material or surface treatment.

The mechanisms involved are variously oxidative, adhesion, abrasion, surface fatigue and plastic deformation. The dominance is controlled by stress, sliding conditions, impact energy, and the difference in material properties, particularly those of plastic deformation, between the two surfaces. There is a paucity of published work that solely investigates and characterises the fundamentals of impact wear.

Impact wear test apparatus falls into two groups; projectiles propelled into a stationary target/specimen, or a target/specimen being repeatedly struck by a hammer. The former type is similar to that commonly used for erosive wear, so the reciprocating hammer/striker type design, was chosen for analysis here.

Analysis was performed on specimens with impact wear scars that feature both material displacement and material loss, enabling comparison between different measurement techniques to be made. This provides a protocol for easier comparison of data, promoting improved models, and furthers the understanding of the apparatus' performance.

1. Introduction

Classically, repetitive (or percussive, or hammering) impact wear of metals is said to be caused by one or more of the primary wear mechanisms removing material from the surface. This damage is responsible either solely, or in part, for the failure of common engineering components and is of particular interest to researchers investigating automotive valvetrains [1–4], wheel-rail contacts [5], power generation [6,7], and mining equipment [8,9]. Some authors have worked at a more fundamental level, but typically focus on the impact wear of a particular type of material [9–13] or surface treatment system [14–18], albeit often with a broad application in mind.

The wear mechanisms involved in the impact wear of metals are variously oxidative, adhesion, abrasion, surface fatigue and plastic deformation [19]. The relative dominance of a particular mechanism is thought to be controlled by the stress, sliding conditions, magnitude of impact energy, and the difference in material properties, particularly those linked to plastic deformation, between the two surfaces in contact [20–25]. A common theme in the literature is the subtlety in definition of 'wear' being wear due to material loss from the surfaces in contact and/or wear due to plastic deformation of material away from that contact zone.

It is perhaps this complexity that means attempts to model impact wear are relatively rare. An initial approach [26] proposed a two-stage model where an 'induction period' in which deformation occurs and a wear scar is formed, but there is no measurable material loss, an idea further explored more recently by the authors of the work presented here [27], and this leads to a 'zero wear limit'. Most mechanical engineering components would continue to operate as intended during the induction period, but once past the zero-wear limit, and into the second stage 'measurable wear region', material loss through the wear mechanisms identified earlier would eventually likely lead to failure.

Subsequent work has either used an Archard type wear law [28] or relationships derived from studies of erosion [29] to develop semi-empirical models to predict the measurable wear and these ideas have been combined to form a compound impact wear model, validated against data from the work of others available in the literature, that is not dependent on the contact geometry [30]. Recent work by the authors of the analysis presented here proposed a model that included consideration of shear force and thus can predict wear due to both

* Corresponding author.
E-mail address: tom.slatter@sheffield.ac.uk (T. Slatter).

https://doi.org/10.1016/j.wear.2023.204816
Received 11 October 2022; Received in revised form 5 February 2023; Accepted 6 February 2023
Available online 29 March 2023

normal and compound impacts [31] and has enabled development of an inverse Gaussian process-based bidirectional model [32]. Others have deduced a purely energy-based wear law from observations that wear is proportional to energy loss during impacts [33] or used finite element modelling approaches [34].

There appears to be a paucity of published work attempting to solely investigate and characterise the fundamental nature of impact wear, particularly when compared to primary wear mechanisms such as abrasion and adhesion. Previous authors have studied the effect of specimen stiffness [35], impact angle [36,37], subsurface changes [38], changes in surface topography [39], and contact lubrication state [40].

Test apparatus designed to assess the impact wear resistance of a particular material or object falls into one of two groups; projectiles being propelled into a stationary target/specimen by various means, be they by gravity [41], a fluid stream [42–44], or magnetic fields [22,45], or a target/specimen is repeatedly struck by a rotating or oscillating hammer driven by various mechanical or electro-mechanical means [13, 24, 46–50]. The former style of apparatus, when used with multiple projectiles being continually propelled (e.g. the aluminium oxide particles entrained in a gas jet in ASTM Standard Test Method G76), is more suitable to the study of erosive wear, because the wear attributed to each individual impact is difficult to discern. When used with single projectiles, this type can also achieve much higher impact velocities more easily than those using a hammer [12], but at the expense of practical difficulties associated with accumulation of repeated impacts in the same contact zone. Considering these points, a reciprocating hammer/striker type design, therefore was chosen for analysis in this repetitive impact wear focussed work.

This study aims to add to the knowledge in this area by presenting analysis of the apparatus when used to subject a number of different metallic specimens to various repetitive percussive impacts. Experiments were carried out at such parameters to generate wear scars that feature both material displacement and material loss, enabling comparison between different measurement techniques to be made. This type of analysis is very rarely found in the formal literature [50] and, although one can often infer that authors have similarly considered their own apparatus in the course of a particular study, it does not appear to have typically been carried out more routinely for the sake of the analysis in and of itself.

It is intended that this work provides a protocol, or suggested methodology, upon which other researchers can base their studies to enable easier comparison of data, thus promoting the development of improved models for impact wear, and also furthers the understanding of the performance of this type of apparatus.

2. Experimental methodology

2.1. Impact test apparatus

In order to have control over the desired parameters, new test apparatus was designed, in a modular fashion, to minimise complexity and to allow many different strikers and specimens to be used. The basic design is an oscillating arm driven by a helical compression spring/cam system, in a third class lever layout, powered by a variable speed/frequency electric motor. A general schematic is shown in Fig. 1 where the elements that are configurable to suit a particular test are highlighted in grey. The configurable components were designed to ensure that, regardless of which were selected to be used for a particular test, the position in three-dimensional space at which the specimen is held does not change. It follows that if the same design of specimen is used, then the surface upon which the impact is first applied is also in the same place for the different configurations of the apparatus. It should be noted, however, that as is the case with many designs of wear testing apparatus, as soon as measurable wear occurs the contact point is likely to be in a different place. Apparatus users should therefore consider if this changes the contact conditions being investigated significantly. In the case of this work, the magnitude of the change in position (microns e.g. the depth of wear scar) is much smaller than the magnitude of the other parameters (millimetres e.g. size of the striker, sizes of the machine elements of the impacting mechanism) therefore it can be considered that the striker impacts the specimen at the same point in space and with the same effective mass.

The main test parameters that can be controlled are; striker-specimen impingement angle (by changing the specimen and striker holders), contact geometry (by changing the form of the striker and specimen as required), and the 'size' of the impact (frequency, force magnitude, velocity/energy, by manipulating in combination; motor rotational speed, spring stiffness, effective mass of arm, cam lift, cam-arm clearance). Other parameters such as temperature, atmosphere, and lubrication state can easily be included by means of simple accessories. Since its original design and commissioning [47] the apparatus has been successfully used for a number of other, more applied, studies [2,7,17,

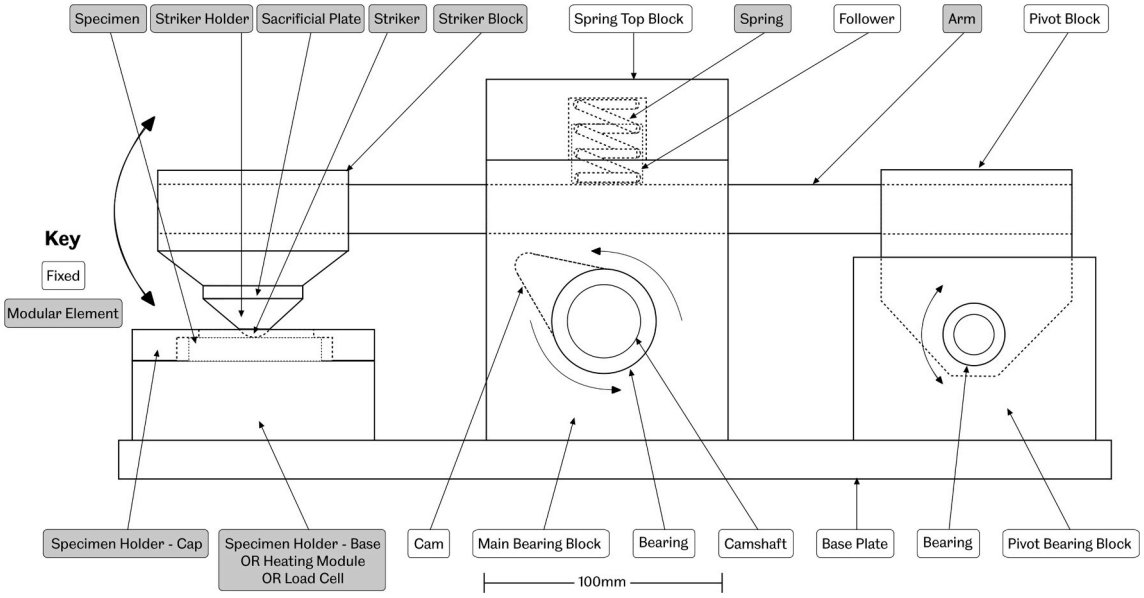

Fig. 1. Schematic of the impact test apparatus.

52,53] in addition to the fundamental work highlighted earlier [27,31].

2.2. Experimental procedure

Throughout this work, whether tests were being performed to primarily analyse the test apparatus itself, as here, or primarily to generate wear scars, as for the work described in Section 3, the following general test set-up was used.

The apparatus is driven by a 1.1 kW electrical motor regulated by a variable frequency controller (inverter) to provide nominal impact frequencies in the range 0–10Hz (i.e. 0-10 impacts per second). The lever arm was driven mechanically by means of a solid cam-follower-spring arrangement and the cam lift was fixed for this work at 5 mm. The same type of helical compression spring, with a stiffness of 29.25 N/mm, was used throughout, its suitability having been established via means of high speed video analysis, similar to that described in Section 2.4.2, that the magnitude of impact energy applied to the specimen is very insensitive to the stiffness of spring that could realistically be used in this apparatus. This spring has been shown to provide stable operation of the apparatus in the other applied studies it has been used for.

The striker at the end of the lever arm was a 15 mm diameter AISI 52100 chrome steel ball with a maximum surface roughness (R_A) of 0.125 μm, a diameter tolerance of ±5 μm, and a sphericity of 5 μm. AISI 52100 is a common bearing steel with high hardness (typically 700–900 HV20) and yield stress (typically 2000 MPa) and therefore, by design, the striker used in this work has over three times the hardness of any of the materials intended to be tested. This means that the damage arising from the impact(s) occurs to the specimen rather than the striker and is thus easier to measure. This is particularly important when using optical measurement methods as the highly polished and spherical nature of the striker surface is difficult to acquire data from with such techniques. A sacrificial plate made from hardened steel is placed between the ball and the striker block to avoid excessive damage to the striker head and was regularly replaced. A new, clean, striker was used for each test and is secured in the striker holder in such a way that it does not rotate about any axis.

Counterface specimens were manufactured from a range of common and commercially available metallic alloys and were nominally 50 mm diameter round discs with a thickness of 10 mm and a surface roughness (R_A) of 0.5 μm achieved by means of grinding. The grinding direction was noted and all specimens were orientated similarly in the apparatus when tested. Regardless of the actual thickness of the specimen after preparation, the surface of the specimen upon which the striker impacts was always in the same position in space. All specimens were examined before each test and any material or residue remaining from their preparation removed prior to testing (e.g. use of a cleaning agent to remove lubricant residue from their manufacture).

2.3. Theoretical characterisation of impact wear test apparatus

As the arm is driven by a spring/cam system, the discussion of the dynamic response of the test rig begins with the analysis of these two elements in isolation. The theoretical performance of the cam can be derived simply and calculated from the manufacturer design data for the cam profile using the classical kinematic equations of motion. To then make an analytical calculation of the impact producing by the cam when driving the apparatus, the following assumptions must be made.

1. The arm and associated components, excluding the spring, are perfectly stiff so deflections and vibrations can be neglected. In reality, there will be some deflection(s) of the arm and striker, especially at impact with the specimen, which may produce multiple strikes per rotation instead of the intended single strike.
2. The inertia of the arm and striker is ignored so as to assume that the cam is in contact with the arm throughout the rotation of the cam. In reality, the inertia of the arm and striker will cause the arm and cam to temporarily separate as the cam profile begins to fall away and the spring cannot maintain the contact between the two elements.
3. The cam profile is assumed to be identical to that described by the design data. The profile of the cam will gradually change through use, due to the sliding wear in the cam and arm contact, and will change the theoretical kinematics of the system.
4. That the arm and cam remain in contact throughout each cycle at a given operating frequency. In reality, there will be an envelope of operating parameters, bounded by the stiffness of the spring and the kinematics of cam and arm such that one of the following is true:
   a. Cam cannot be rotated fully (frequency too low, spring stiffness too high),
   b. Arm and cam remain in contact throughout (rate at which the cam ‘falls away’ is less than the maximum acceleration of the arm that could be achieved by the spring force),
   c. Arm and cam do not remain in contact, but impact still occurs (rate at which the cam ‘falls away’ is greater than the maximum acceleration of the arm-striker that could be achieved by the spring force alone),
   d. Arm and cam do not remain in contact and impact does not occur (point at which the cam returns to lift the arm for the next cycle is prior to the arm-striker falling enough to cause an impact).

Assuming that the arm has a constant angular velocity throughout its length, the velocity of the striker relative to the cam/arm contact is proportional to the ratio of the distance of the arm pivot to the striker and the arm pivot to the cam. A similar approach can be used to calculate the effective mass of the apparatus for purposes of calculating the kinetic energy of the striker at the point of impact, and for the apparatus being considered here operating at 10 Hz with an arm-cam clearance of 2 mm, is shown in Fig. 2. The point at which the striker initially comes into contact with the specimen on each rotation of the cam (which in this case has a slightly asymmetric geometry due to its original automotive application [2]) is marked on Fig. 2 with a black, dashed line, and with typical operating conditions used in this work the striker impinges onto the surface of the specimen when the cam is at 128°.

2.4. Experimental characterisation of impact wear test apparatus

It is unlikely that a test rig such as this behaves exactly as theorised due to the assumptions made therefore a number of different experimental approaches were used to characterise the actual behaviour of the apparatus and inform a judgement of the robustness of the data it produces.

2.4.1. Force analysis

The dynamic performance of the apparatus was characterised by means of a calibrated, low-profile, pancake type load cell (5 kN load capacity, linearity of ±0.5% of rated output, repeatability of ±0.145% of rated output) placed below the specimen. In this case a stainless steel (AISI 304) specimen was used, but any metallic material would be suitable provided it is used as the counterface throughout any analysis, during tests to measure the impact force during repetitive normal impact at room temperature. The selected load cell can measure the load within the range 5–5000 N which is adequate for the expected forces and the data was acquired by a data acquisition system with a sampling frequency of 4.8 kHz. This was chosen to be sufficiently fast to capture any ‘events’, such as rebounds, within each test cycle (in this presented case of 10 apparatus cycles/nominal impacts per second).

A typical dataset for one apparatus cycle is shown in Fig. 3a, and illustrates the rebounds, or extra impacts, that occur and compares well with the high-speed video analysis (Section 2.4.2). Throughout the dataset, the initial impact force spike occurs every 0.1 s therefore verifying the nominal operating frequency of the apparatus. Force data for 10 s of apparatus operation was regularly collected throughout testing

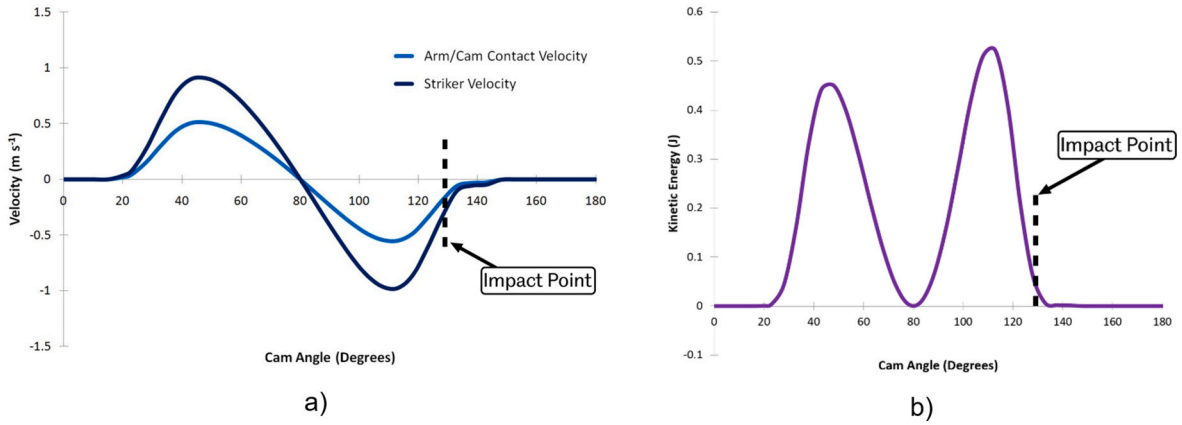

Fig. 2. Cam Angle vs. (a) Calculated Velocity for the Striker and the Arm/Cam Contact, and (b) vs. Calculated Kinetic Energy for the Striker.

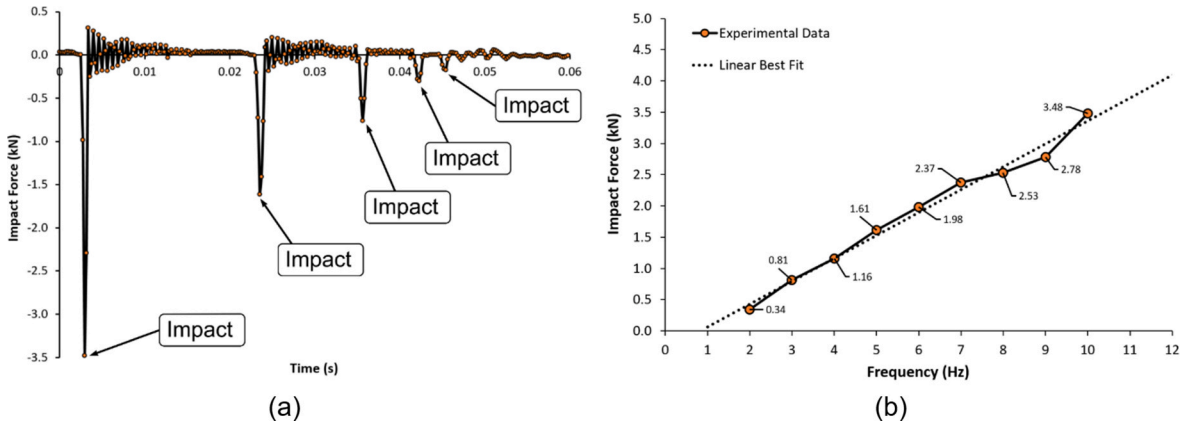

Fig. 3. (a) Impact force(s) data for a single nominal impact at an apparatus operating frequency of 10 Hz, (b) Initial impact force value at different apparatus operating frequencies.

and the mean peak impact force and rebound impact forces were recorded. In the cycle shown in Fig. 3a, the initial impact was 3476 N, with the subsequent four rebounds being 1507 N, 509 N, 295 N, and 170 N. This analysis was repeated to confirm the level of impact force at different nominal operating frequencies that apparatus of this type has previously been shown be stable [51,54]. The mean peak values (standard deviation of 8.8) of initial impact force obtained by the load cell during testing at various nominal apparatus operating frequencies in the range 2–10 Hz are shown in Fig. 3b. All tests performed showed four rebounds during impact based on the impact force analysis which also confirms the stability of rig within this range. It is important to perform this type of experimental analysis as the contact (dynamic, plastic) is beyond the usually accepted limits of classical Hertzian approach (static, elastic).

2.4.2. *High-speed video analysis*

High-speed video recording was utilised to investigate the actual behaviour of the apparatus when it is operating. For the majority of the experimental characterisation, all parameters of the apparatus were held as per the theoretical characterisation, other than the angle of impact. A solid aluminium block, in this example (Fig. 3a) of 30° inclination, was used in place of a specimen holder and specimen to maintain line of sight between the striker impact zone and the camera that would otherwise be obscured (Fig. 4a). The framerate of the video camera was set to be two orders of magnitude higher than the frequency of impact (in this case 1000 fps) to adequately capture the motion, in particular the rebounds. Analysis of the recorded images can reveal the actual displacements that the components undergo during operation (Fig. 4b). To achieve this, the footage was analysed using motion-tracking software and an example for 2½ cam rotations, or 0.25s of running time, series of normal impacts and their associated displacements.

It is clear from Fig. 4c that, as with the normal impacts used as an example of force analysis (Section 2.4.1), there are multiple impacts on the 'specimen' per rotation of the cam and that they decrease in amplitude. It also follows that the velocities and accelerations behave correspondingly assuming they are derived from the displacement data.

The captured footage also revealed that both the number of extra impacts per cam rotation and the initial rebound height magnitude is constant for a particular spring, but varies with spring stiffness, appearing to be greater with a softer spring, indicating that spring stiffness is a system controlling parameter. Even though by design the point of impact is always at the same point in space, irrespective of any particular test, the height of the first 'rebound' for impacts occurring up to 45° from normal are two thirds that of the initial rebound from a normal impact.

It is also apparent that the ability of the spring to resist the inertia of the arm/striker system varies with stiffness and the arm can leave the cam momentarily as the nose passes. The cam only effectively controls the vertical component translation of the arm rather the entire translation. The effect of this phenomenon is that the effective height from which the striker falls can be greater than intended, particularly if the spring is less stiff than required and cannot maintain the arm-cam contact (as described in Section 2.3).

As expected, the dynamic behaviour of the test rig is different to that theorised. From the cam design data, the calculated (as described in

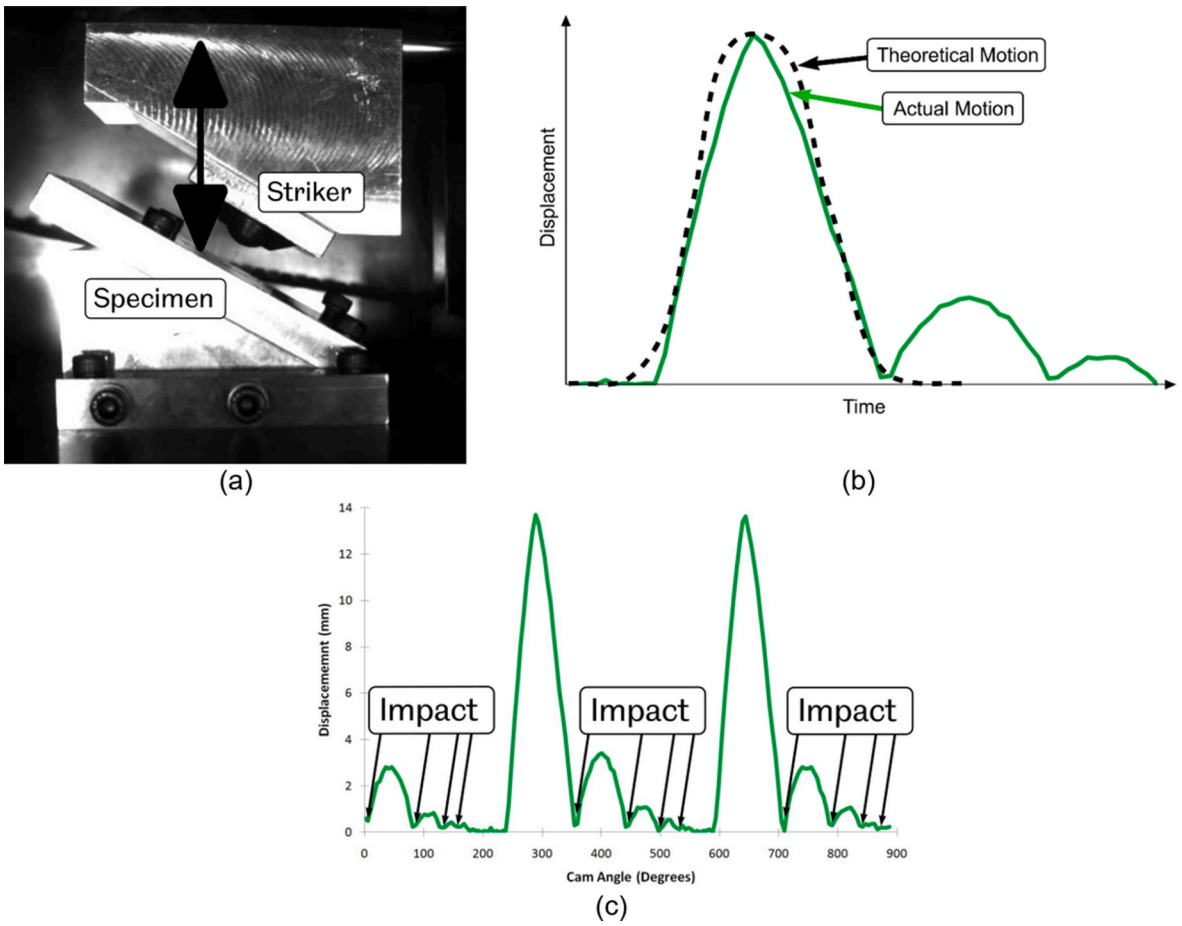

Fig. 4. (a) Example high speed video frame, and analysis; (b) comparison of actual and theoretical motion, (c) cam angle vs. displacement of striker from high speed video capture for a 30° inclination impact.

Section 2.3) velocity of the striker just before impact is 0.51 m s^{-1} whereas the experimental results showed that, on average for the first impact of all tests, the equivalent velocity was 0.45 m s^{-1}. This reduced value naturally leads to a similar discrepancy in the values for the kinetic energy of the striker as it impacts the specimen, calculated to be on average 0.22J rather than 0.28J. Taking the extra rebounds as extra impacts per rotation of the cam the total energy imparted into the specimen by the striker per cycle in this instance can be calculated to be 0.7J. Ultimately, the energy loss in the system, between the theoretical and experimental values, is predominately caused by friction in the cam-arm-spring system and is lost as heat.

The high-speed video footage was also used to investigate the distance that the striker slides against an inclined specimen surface during an impact. Due to the small distances observed it was only realistic to obtain values for the sliding due to the first impact in each cycle. Five impacts were measured and the average distance a point on the striker slid beyond the initial point of contact for a 30° impact was 0.44 mm and for a 45° impact was 0.72 mm.

3. Impact wear testing

The test apparatus was then used, as described in Section 2.2, for the purpose of generating of wear scars on common metallic materials used in engineering applications with the purpose of validating its operation, and providing a reference for others to do the same, and to propose a measurement method.

The specimens were manufactured from as received round bars of; a ductile cast iron (EN-GJS-600-3), a medium carbon steel (EN8), an austenitic stainless steel (304), a phosphor bronze (PB102), and an aluminium alloy (AlSi9Cu3).

For the purposes of this part of the work, and to reduce the complexity of the Design of Experiment, the test specimens were each subjected to repeated normal impacts a nominal impact frequency (apparatus operating frequency) of 10 Hz for either 60 min (36,000 impacts), 1.5 h (54,000 impacts) or 2 h (72,000 impacts). Four samples of each specimen were used and each test, where a 'test' was one of every test time and material combination, was conducted with a new test specimen and new striker. The worn specimens were photographed and the wear scar geometries recorded after each test. The form and nature of any visible wear debris was also recorded.

4. Wear scar analysis

4.1. Wear scar morphology

The striker was inspected after each test and as expected, there were occasionally superficial witness marks on the surface of the striker, but otherwise no measurable wear.

Fig. 5 shows example test specimens having been subjected to impact and the wear debris visible can vary as shown in the figure by the presence of particles which vary in size and nature. The wear scars can be easily seen by the naked eye and in general the wear scars can be characterised as follows and is in agreement with literature introduced in Section 1, suggesting that this apparatus is consistent with other impact wear generating methods.

Ductile cast iron (EN-GJS-600-3) - a smaller wear scar, well defined edges with significant plastic flow on all edges. Minimal evidence of micro pitting in the centre of wear scar.

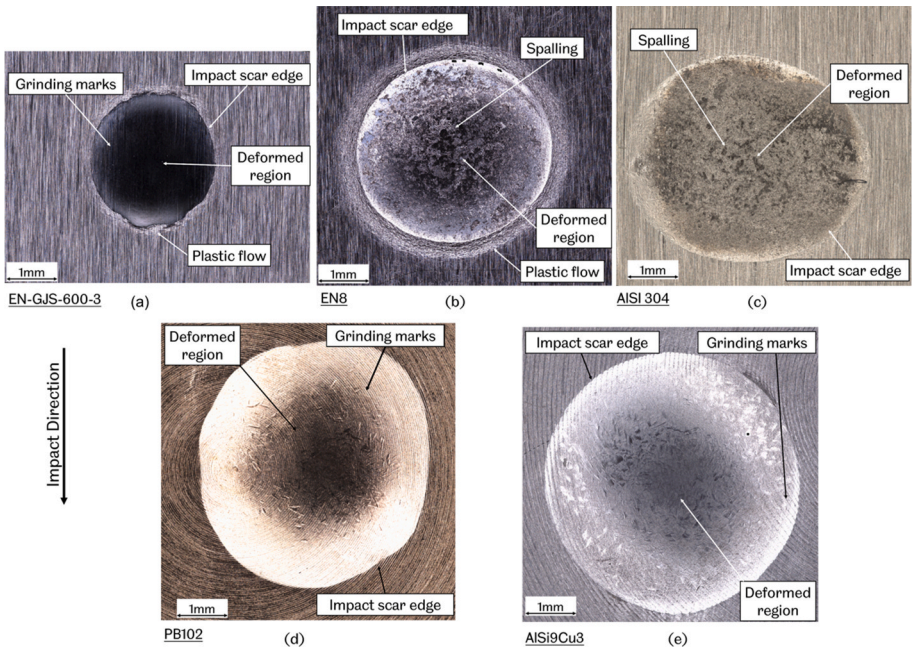

Fig. 5. Typical impact wear scar for tested materials after 36,000 cycles for (a) ductile cast iron (EN-GJS-600-3), (b) medium carbon steel (EN8), (c) austenitic stainless steel (AISI 304), (d) phosphor bronze (PB102), and (e) aluminium alloy (AlSi9Cu3).

Medium carbon steel (EN8) - larger wear scar with well-defined edges and significant plastic flow, microcracks in the centre of wear scar, no evidence of circumferential cracks near the edges.

Austenitic stainless steel (AISI 304) - Smooth, well-defined edges. Scars slightly oval in shape with no evidence of plastic flow on the edges, mostly plastic deformation with pitting (spalling) in the centre of the wear scar.

Phosphor bronze (PB102) and *aluminium alloy (ALSI9Cu3)* - a large wear scar with no evidence of plastic flow on the edges, some evidence of micro pitting in the centre of wear scar and mainly plastic deformation within the wear scar region.

Fig. 6a and b illustrates evidence to identify the wear mechanism in the centre of the impact crater of the austenitic stainless steel and medium carbon steel specimens. In some specimens plastic flow is also evident on the edges of the ductile cast iron (Fig. 6c), aluminium alloy (Fig. 6d), and medium carbon steel below(Fig. 6e) specimens in addition to wear debris and microcracks.

4.2. Wear scar measurement

Measurements, in 2D and 3D, of the wear scars produced by the tests were made to demonstrate the trade-off between cost and complexity for each approach. For the purposes of the analysis presented here, a 3D non-contact profilometer (focus variation type) was used throughout with 2D data derived from the native 3D dataset to avoid errors arising from using more than one instrument. 2D contact profilometry (stylus type) is also used widely in literature, including for work using the specific apparatus used here [2,7,17,51,53], and in industrial practice as it can be an order of magnitude lower in resource costs. The ratio between test specimen size and wear scar size means that mass loss methods are impractical and the non-use of which is a sacrifice against reasonable test length (to produce a wear scar suitable for measurement by mass loss) and specimens that can contain the sub-surface stress field resulting from each impact within their volume.

4.2.1. 2D measurement of wear scar geometry

Three different 2D profiles taken across the centre of the wear scar were produced from the full 3D datasets acquired of the surfaces of each tested specimen and a typical profile for a wear scar on each material after 36,000 impacts is shown in Fig. 7. The instrument software (MeasureSuite) was used to set a reference plane for each dataset corresponding to the ground surface of the specimen. Diametric measurements were produced for wear scars present on each of the specimens and the averages (with standard deviations of 0.30 (AlSi9Cu3), 0.38 (Pb102), 0.16 (AISI 304), 0.44 (EN8), 0.10 (EN-GJS-600-3)) of these are shown in Fig. 8 (circular datapoint markers, "Dia."). Depth measurements corresponding to these diameter measurements were also made to later assess the depth of the wear scar for purposes of estimating the wear volume (Section 4.2.2). This data was also previously used by the authors to investigate the zero wear phenomenon [27].

Fig. 7 reveals, in general, the smooth surface profile of the materials' craters and the results confirm the loss of small amounts of material as wear debris. The medium carbon steel and ductile cast iron clearly have obvious plastic flow (pile-up) on the 'shoulders' of the impact scar. The aluminium alloy has some plastic flow, but there is no plastic flow apparent for either the austenitic stainless steel or the phosphor bronze.

Fig. 8 shows that the ductile cast iron, which has the highest hardness, has a diameter approximately 40% less than that of ALSi9Cu3. This illustrates the role of hardness, providing approximately similar readings of impact wear crater diameters for all specimens except those manufactured from ductile cast iron due to their similar hardness, and the consideration of work hardening when carrying out tests such as these.

4.2.2. Use of 2D profilometry data for wear scar volume estimation

Fig. 8 also presents calculated estimates (diamond data point markers, "Calc. Vol.") of wear scar volume. The average values of the directly measured wear scar geometry, the depth and the diameter, also were used as the basis of a geometrical calculation. If it is assumed that the general shape of a wear scar is one of a of a sphere partially moved into the general plane of the surface of the test specimen, then the spherical cap relationship given by Equation (1) gives a good approximation of the wear scar volume:

$$V = \frac{\pi h\left(3a^2 + h^2\right)}{6} \qquad \text{Equation 1}$$

where, V represents the estimated wear scar volume (mm^3) derived from

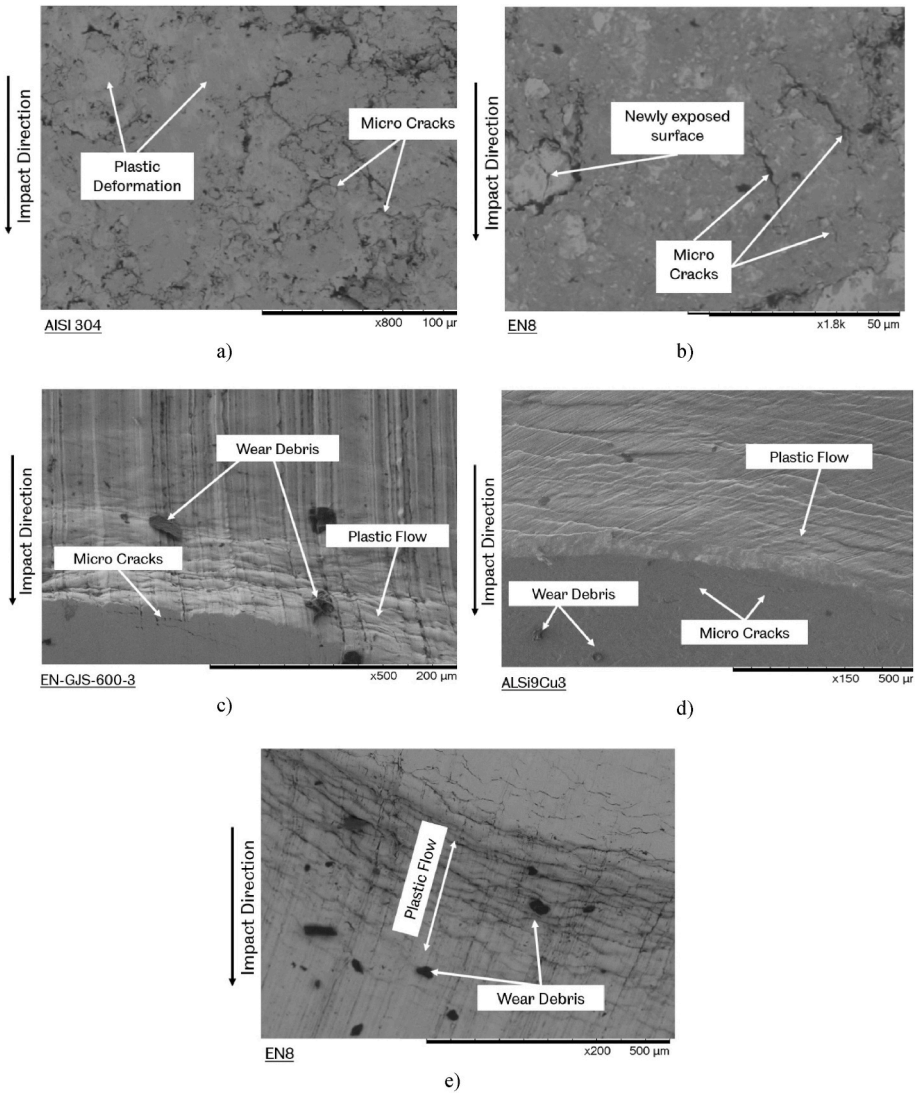

Fig. 6. Damage mechanism in the centre of the impact scar on the (a) austenitic stainless steel (AISI 304) and (b) the medium carbon steel (EN8), and plastic flow formation on the edges and microcracks of (c) ductile cast iron (EN-GJS-600-3) (d) aluminium alloy (AlSi9Cu3), (e) medium carbon steel (EN8), after 36,000 cycles.

the measured average wear scar depth (h, mm) and measured average wear scar radius (a, mm).

4.2.3. 3D measurement of wear scar geometry

The datasets obtained from the non-contact profilometer were also used to perform a 3D analysis and the data for a typical wear scar for each material tested is shown in Fig. 9. This method provides clear illustration beyond that of the 2D analysis of the lip or ridges formed by the deformed material and the typical difference in wear scar size between the different materials.

The data in Fig. 9 confirms that presented in Fig. 7 in that both the phosphor bronze and aluminium alloy have the highest depth (blue colour in Fig. 9) in the centre of the impact crater, while ductile cast iron has the lowest depth, thereby showing the role played by material hardness and consideration of where and what the "diameter" of the wear scar measured in 2D actually represents.

The total volume loss was also calculated measured by using through direct volume measurement method in the 3D non-contact profilometer software (MeasureSuite), the results of which are also shown in Fig. 8 (square datapoint markers, "Vol."), with standard deviations of 0.510 (AlSi9Cu3), 0.600 (Pb102), 0.136 (AISI 304), 0.270 (EN8), 0.026 (EN-GJS-600-3).

5. Discussion

In general, the wear mechanisms observed were as suggested by previous authors [25] confirming the ability of the test apparatus to repeatability produce wear from normal impacts representative of that observed and reported elsewhere. Where there is a high impact velocity, which is considered to be the case throughout this work, and therefore high impact energy, if there is a soft material in the contact plastic deformation occurs with ductile extrusion away from the contact. The 'softer' materials exhibited smooth wear scar edges further supporting the presence of this wear mechanism. Care should be taken to consider the specific microstructure of the materials under investigation.

The hardest material tested, the ductile cast iron, exhibited rougher edges to the wear scars compared to the other materials. This indicates that brittle fracture is beginning to take place. If high energy impacts occur on a brittle surface, there is little plastic deformation as described previously and fracture occurs. The large, metallic flakes visible after test performed using the lamellar graphite cast iron are as expected given the microstructure of the material and further support the fracture mechanism demonstrated here.

Examination of damage mechanisms by scanning electron microscopy (SEM) and 3D non-contact profilometer revealed that the main damage mechanism for the tested materials was mainly plastic

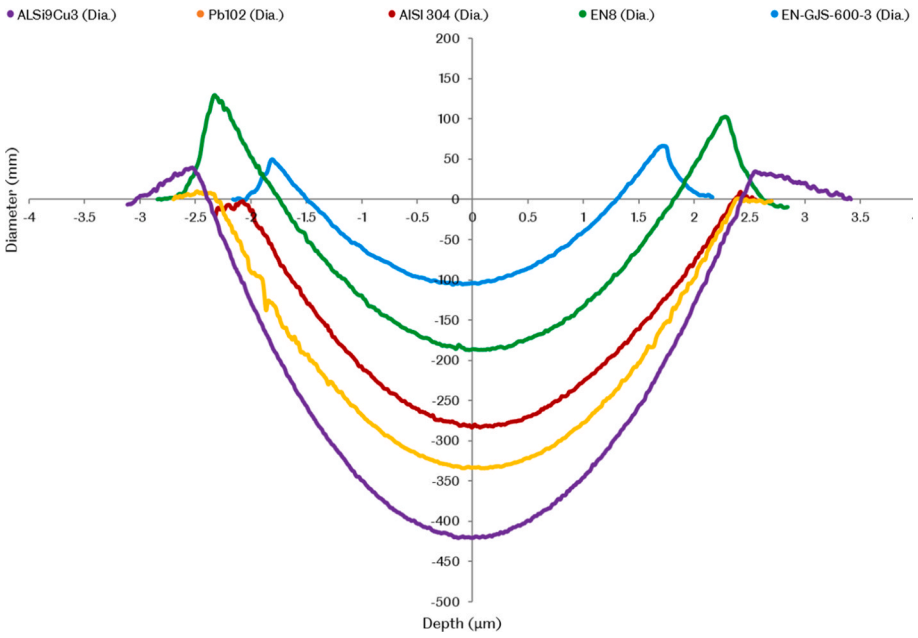

Fig. 7. Typical single 2D diametric wear scar profiles after 36,000 cycles.

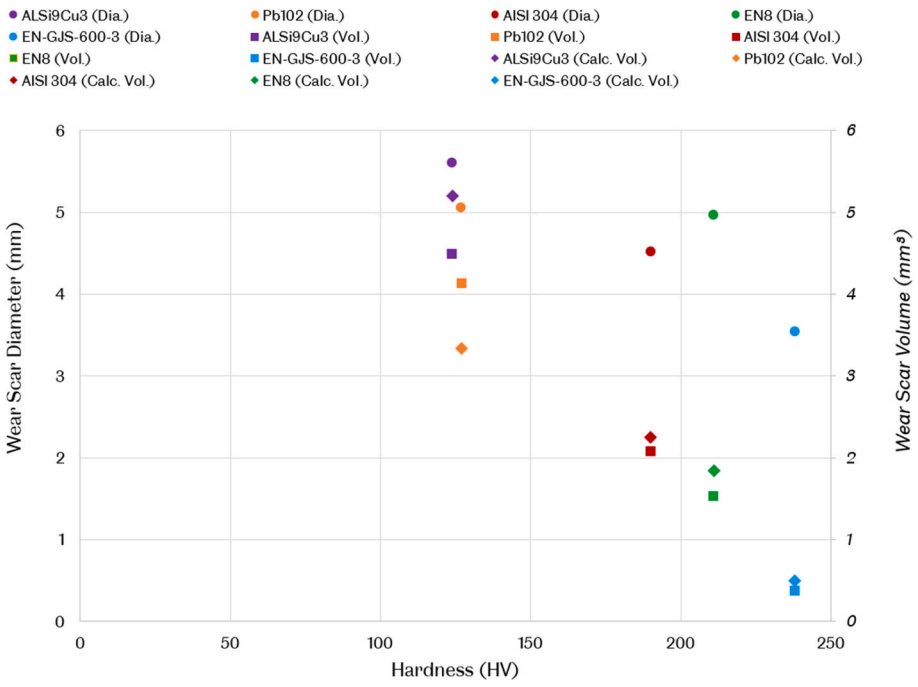

Fig. 8. Directly measured wear scar diameters and volumes, and calculated volumes.

deformation and surface fatigue due to spalling as a result of small pitting and microcracks. There was no obvious delamination or material transfer to the striker (ball) surface observed in any of the tests. It is these characteristic features that should be identified when comparing work from different sources to ensure proper comparison.

Ultimately the ability of a material to resist plastic deformation contributes to its wear performance therefore it may be instructive to investigate the proportion of the material that is plastically 'worn away' from the loaded area, in addition to totally removed (or lost) from the contact area as wear debris. This 'zero wear volume' concept is further discussed elsewhere [27] by the authors of this analysis.

The apparatus used here was found to work in good operation in the frequency range tested and there is direct linear correlation between the impact force and frequency. This should not be taken as always being true and users should conduct similar studies to ascertain the exact number of rebounds that occur. This will particularly be true as apparatus operating frequencies increase such that the impactor drive mechanism, in this case a cam, completes its cycle of operation before the impactor has rebounded, and eventually will not strike the specimen at all. The data from the 2D measurements of wear scar diameter (Fig. 8, circular data markers) suggests that higher hardness generally results in improved wear resistance, as one would expect for conventionally processed metallic engineering alloys such as those tested here. The distribution of this data is affected by the difficulty in achieving consistent

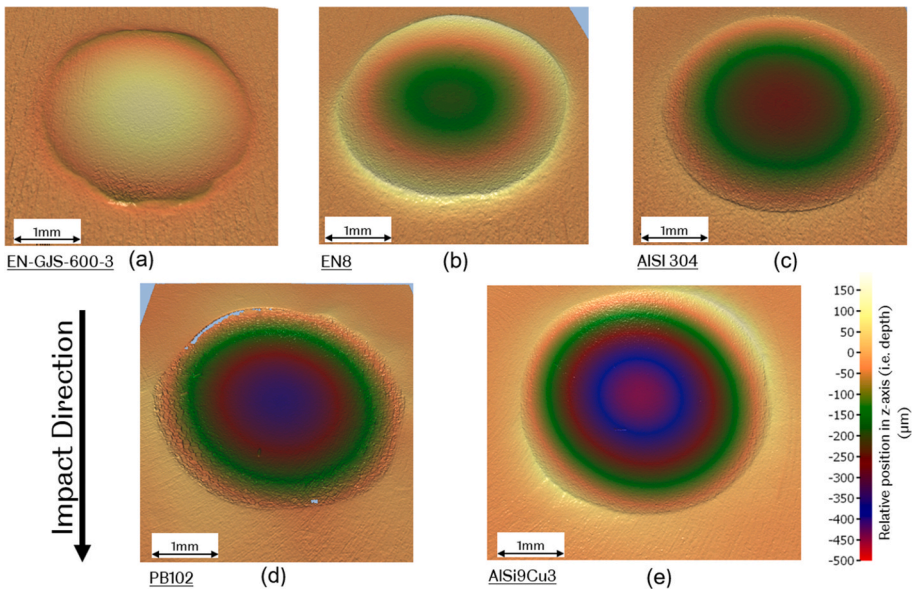

Fig. 9. Typical (largest) wear scars for (a) ductile cast iron (EN-GJS-600-3), (b) medium carbon steel (EN8), (c) austenitic stainless steel (AISI 304), (d) phosphor bronze (PB102), and (e) aluminium alloy (AlSi9Cu3).

reference points for measurement of the diameters of wear scars produced on materials with differing levels of ductile extrusion 'shoulders' (as illustrated in Fig. 7) and thus reduces its quality. Similarly, it is also difficult to ensure the measured diameters on a single wear scar cross at the true centre of maximum wear scar depth.

This also impacts the quality of the wear volume loss data calculated from those diameters (Fig. 8, diamond data markers). There is a potential 'area of uncertainty' at the bottom of the wear scar that is hard to quantify and as both the wear scar diameter (as a radius) and depth are squared in Equation (1) the uncertainty can become quite large for the final calculated wear loss volume.

When compared with the data representing the directly measured wear volumes (Fig. 8, square data markers), and assuming this data is more 'accurate', it is interesting to note that for the higher hardness materials tested the difference between the directly measured and calculated volumes is much smaller than for the lower hardness materials. When considering these trends with the typical wear profiles shown in Fig. 7, there appears to be no clear evidence of the mechanism behind this, but it is suggested that it is a result of the synergy, or not, of the ductility of the material and the level of zero wear for that material. Data from the investigation into zero wear [27] suggests that the proportion of the total wear loss due to zero wear for ductile cast iron (~30%) and the medium alloy steel (~50%) is much lower compared to the stainless steel (~95%) for the same test conditions as used in this work. The stainless steel has lower hardness than the ductile cast iron and medium alloy steel, and these two properties interact, bringing the direct and calculated volume losses closer together. The specific nature of the impact wearing occurring for a particular material should therefore be taken onto account when selecting a measurement method.

6. Conclusions

The aim of this work was to provide analysis of reciprocating hammer type impact wear apparatus in such a way as to provide conclusions that inform and guide the users of similar equipment, thus.

1) Impact wear apparatus should be characterised to understand the actual number and nature of impacts it is imparting on a specimen surface.
2) For most harder metallic materials, simple 2D (contact or non-contact) profilometry is adequate to produce a representative ranking of impact wear resistance. For softer metallic materials 3D non-contact profilometry should be considered.
3) If 2D profilometry is used, care should be taken to ensure measurement reference points are consistent for repeated wear scar diameter and depth measurements of a single scar and measurements of wear scars produced of different specimens.
4) The mechanical properties of materials to be tested, and their likely response in terms of the classical modes of impact wear, should be considered prior to selecting test and measurement methods.

This work also serves as a suggested analysis methodology and reference for others working in impact wear to enable easier comparison of experimental data and promotes rigorous validation of impact wear models. It also highlights the importance of analysing carefully how impact wear apparatus is performing during use that could lead to misinterpretation of results.

Declaration of competing interest

The authors declare that they have no known competing financial interests or personal relationships that could have appeared to influence the work reported in this paper.

Acknowledgements

The authors gratefully acknowledge the kind support of: Engineering & Physical Sciences Research Council (CASE/CNA/04/05 SRDE0004a) (financial support of TS), Iraqi Ministry of Oil and LUKOIL (financial support of MZ).

References

[1] S.D.A. Lawes, S.V. Hainsworth, M.E. Fitzpatrick, Impact wear testing of diamond-like carbon films for engine valve-tappet surfaces, Wear 268 (Issue 11) (2010) 1303–1308, https://doi.org/10.1016/j.wear.2010.02.011. ISSN 0043-1648.
[2] T. Slatter, H. Taylor, R. Lewis, P. King, The influence of laser hardening on wear in the valve and valve seat contact, Wear 267 (Issue 5) (2009) 797–806, https://doi.org/10.1016/j.wear.2009.01.040. ISSN 0043-1648.
[3] T. Ootani, N. Yahata, A. Fujiki, A. Ehira, Impact wear characteristics of engine valve and valve seat insert materials at high temperature (impact wear tests of austenitic heat-resistant steel SUH36 against Fe-base sintered alloy using plane specimens), Wear 188 (Issue 1) (1995) 175–184, https://doi.org/10.1016/0043-1648(95)06656-X. ISSN 0043-1648.

[4] R. Lewis, R. Dwyer-Joyce, G. Josey, Investigation of wear mechanisms occurring in passenger car diesel engine inlet valves and seat inserts, Technical Paper 1999-01-1216, SAE, 1999, https://doi.org/10.4271/1999-01-1216.

[5] W.J. Jiang, C. Liu, C.G. He, J. Guo, W.J. Wang, Q.Y. Liu, Investigation on impact wear and damage mechanism of railway rail weld joint and rail materials, Wear 376–377 (Part B) (2017) 1938–1946, https://doi.org/10.1016/j.wear.2017.02.035. ISSN 0043-1648.

[6] S.-S. Chang, H.-C. Wu, C. Chen, Impact wear resistance of stellite 6 hardfaced valve seats with laser cladding, Mater. Manuf. Process. 23 (7) (2008) 708–713, https://doi.org/10.1080/10426910802317102.

[7] T. Bruce, H. Long, T. Slatter, R. Dwyer-Joyce, Formation of white etching cracks at manganese sulfide (MnS) inclusions in bearing steel due to hammering impact loading, Wind Energy 19 (2016) 1903–1915, https://doi.org/10.1002/we.1958.

[8] R.W. Fricke, C. Allen, Repetitive impact wear of steels, Wear 162 (1993) 837–847, https://doi.org/10.1016/0043-1648(93)90085-Z. ISSN 0043-1648.

[9] Y.-Y. Yang, H.-S. Fang, Y.-K. Zheng, Z.-G. Yang, Z.-L. Jiang, The failure models induced by white layers during impact wear, Wear 185 (Issue 1) (1995) 17–22, https://doi.org/10.1016/0043-1648(94)06586-1. ISSN 0043-1648.

[10] S.L. Rice, H. Nowotny, S.F. Wayne, Characteristics of metallic subsurface zones in sliding and impact wear, Wear 74 (Issue 1) (1981) 131–142, https://doi.org/10.1016/0043-1648(81)90199-X. ISSN 0043-1648.

[11] G. S Zhang, J.-D. Xing, Y.-M. Gao, Impact wear resistance of WC/Hadfield steel composite and its interfacial characteristics, Wear 260 (Issue 7) (2006) 728–734, https://doi.org/10.1016/j.wear.2005.04.010. ISSN 0043-1648.

[12] M. Lindroos, V. Ratia, M. Apostol, K. Valtonen, A. Laukkanen, W. Molnar, K. Holmberg, V.-T. Kuokkala, The effect of impact conditions on the wear and deformation behavior of wear resistant steels, Wear 328 (2015) 197–205, https://doi.org/10.1016/j.wear.2015.02.032. ISSN 0043-1648.

[13] R. Kumar, M. Antonov, P. Klimczyk, V. Mikli, D. Gomon, Effect of cBN content and additives on sliding and surface fatigue wear of spark plasma sintered Al2O3-cBN composites, Wear 494–495 (2022), 204250, https://doi.org/10.1016/j.wear.2022.204250.

[14] K.-D. Bouzakis, M. Batsiolas, G. Skordaris, F. Stergioudi, N. Michailidis, Repetitive impact test near uncoated and coated cutting edges for assessing their fatigue behavior, CIRP J. Manuf. Sci. Tech. 8 (2015) 63–69, https://doi.org/10.1016/j.cirpj.2014.09.001.

[15] K.-D. Bouzakis, P. Charalampous, G. Skordaris, F. Dimofte, N.M. Ene, R. Ehinger, S. Gardner, B.S. Modrzejewski, J.R. Fetty, Fatigue and adhesion characterization of DLC coatings on steel substrates by perpendicular and inclined impact tests, Surf. Coating. Technol. 275 (2015) 207–213, https://doi.org/10.1016/j.surfcoat.2015.05.018.

[16] R. Bantle, A. Matthews, Investigation into the impact wear behaviour of ceramic coatings, Surf. Coating. Technol. 74 (1995) 857–868, https://doi.org/10.1016/0257-8972(95)08314-6. ISSN 0257-8972.

[17] T. Slatter, R. Lewis, A.H. Jones, The influence of cryogenic processing on wear on the impact wear resistance of low carbon steel and lamellar graphite cast iron, Wear 271 (Issue 9) (2011) 1481–1489, https://doi.org/10.1016/j.wear.2011.01.041. ISSN 0043-1648.

[18] Y. Ren, P. Wang, Z. Cai, J. He, J. Lu, J. Peng, X. Xu, M. Zhu, Dynamic response characteristics and damage mechanism of impact wear for deep plasma nitride layer, Tribol. Int. 170 (2022), 107496, https://doi.org/10.1016/j.triboint.2022.107496.

[19] P.A. Engel, Percussive impact wear, Tribol. Int. 11 (Issue 3) (1978) 169–176, https://doi.org/10.1016/0301-679X(78)90002-6. ISSN 0301-679X.

[20] E. Rabinowicz, Metal transfer during static loading and impacting, Proc. Phys. Soc. B 65 (8) (1952) 630, https://doi.org/10.1088/0370-1301/65/8/313.

[21] R.S. Montgomery, The mechanism of percussive wear of tungsten carbide composites, Wear 12 (Issue 5) (1968) 309–329, https://doi.org/10.1016/0043-1648(68)90535-8. ISSN 0043-1648.

[22] R.G. Bayer, P.A. Engel, J.L. Sirico, Impact wear testing machine, Wear 19 (Issue 3) (1972) 343–354, https://doi.org/10.1016/0043-1648(72)90125-1. ISSN 0043-1648.

[23] G. Laird, Repetitive- and single-blow impact testing of wear-resistant alloys, J. Test. Eval. 23 (No. 5) (1995) 333–340, https://doi.org/10.1520/JTE11402J. ISSN 0090-3973.

[24] C.J. Studman, J.E. Field, A repeated impact testing machine, Wear 41 (Issue 2) (1977) 373–381, https://doi.org/10.1016/0043-1648(77)90015-1. ISSN 0043-1648.

[25] G.W. Stachowiak, A.W. Batchelor, Engineering Tribology, Butterworth Heinemann, Boston, 2005.

[26] P.A. Engel, Impact Wear of Materials, Elsevier, Amsterdam, 1976.

[27] M. Zalzalah, R. Lewis, T. Slatter, Defining the role of 'zero wear volume' in percussive impact, Wear 464–465 (2021), 203535, https://doi.org/10.1016/j.wear.2020.203535.

[28] E. Rabinowicz, K. Hozaki, Impact wear of ductile metals, Proceed. JSLE Int. Tribol. Conf. 2 (1985, July) 263–268.

[29] R.W. Fricke, C. Allen, Repetitive impact wear of steels, Wear 162 (1993) 837–847, https://doi.org/10.1016/0043-1648(93)90085-Z. ISSN 0043-1648.

[30] R. Lewis, A modelling technique for predicting compound impact wear, Wear 262 (Issue 11) (2007) 1516–1521, https://doi.org/10.1016/j.wear.2007.01.032. ISSN 0043-1648.

[31] M. Zalzalah, R. Lewis, T. Slatter, A New Predictive Model for Normal and Compound Impact Wear, vols. 480–481, Wear, 2021, 203954, https://doi.org/10.1016/j.wear.2021.203954.

[32] F. Lou, Z. Ma, S. Nie, H. Ji, F. Yin, A bidirectional wear model based Inverse Gaussian (IG) process for PEEK against AISI630 stainless steel in seawater hydraulic components, Tribol. Int. 175 (2022), 107815, https://doi.org/10.1016/j.triboint.2022.107815.

[33] T. Souilliart, E. Rigaud, A. Le Bot, C. Phalippou, Energy-based wear law for oblique impacts in dry environment, Tribol. Int. 105 (January) (2017) 241–249, https://doi.org/10.1016/j.triboint.2016.10.014. ISSN 0301-679X.

[34] G. Skordaris, K.-D. Bouzakis, P. Charalampous, A dynamic FEM simulation of the nano-impact test on mono- or multi-layered PVD coatings considering their graded strength properties determined by experimental–analytical procedures, Surf. Coating. Technol. 265 (2015) 53–61, https://doi.org/10.1016/j.surfcoat.2015.01.063.

[35] S.L. Rice, H. Nowotny, S.F. Wayne, The role of specimen stiffness in sliding and impact wear, Wear 77 (Issue 1) (1982) 13–28, https://doi.org/10.1016/0043-1648(82)90041-2. ISSN 0043-1648.

[36] E. Rigaud, A. Le Bot, Influence of incidence angle on wear induced by sliding impacts, Wear 307 (Issue 1) (2013) 68–74, https://doi.org/10.1016/j.wear.2013.07.015. ISSN 0043-1648.

[37] W.R. Tyfour, M.T. Hayajneh, R. Hendawi, Role of impact angle reversal on impact wear of mild steel, Proc. IME J. J. Eng. Tribol. (2017), https://doi.org/10.1177/1350650117705978.

[38] S. L Rice, H. Nowotny, S.F. Wayne, Formation of subsurface zones in impact wear, Asle Trans. 24 (2) (1981) 264–268, https://doi.org/10.1080/05698198108983020.

[39] P.A. Engel, D.B. Millis, Study of surface topography in impact wear, Wear 75 (Issue 2) (1982) 423–442, https://doi.org/10.1016/0043-1648(82)90162-4. ISSN 0043-1648.

[40] P.A. Engel, J.L. Sirico, Impact wear study of lubricated contacts, ASLE Trans. 18 (4) (1975) 279–289, https://doi.org/10.1080/05698197508982770.

[41] K. Wellinger, H. Breckel, Kenngrössen und Verschleiss beim Stoss metallischer Werkstoffe, Wear 13 (Issue 4) (1969) 257–281, https://doi.org/10.1016/0043-1648(69)90249-X. ISSN 0043-1648.

[42] G.L. Sheldon, A. Kanhere, An investigation of impingement erosion using single particles, Wear 21 (Issue 1) (1972) 195–209, https://doi.org/10.1016/0043-1648(72)90257-8. ISSN 0043-1648.

[43] L. Lapides, A. Levy, The halo effect in jet impingement solid particle erosion testing of ductile metals, Wear 58 (Issue 2) (1980) 301–311, https://doi.org/10.1016/0043-1648(80)90159-3. ISSN 0043-1648.

[44] A.K. Cousens, I.M. Hutchings, A critical study of the erosion of an aluminium alloy by solid spherical particles at normal impingement, Wear 88 (Issue 3) (1983) 335–348, https://doi.org/10.1016/0043-1648(83)90302-2. ISSN 0043-1648.

[45] N.J. Mahoney, R.J. Grieve, T. Ellis, A simple experimental method for studying the impact wear of materials, Wear 98 (1984) 79–87, https://doi.org/10.1016/0043-1648(84)90218-7. ISSN 0043-1648.

[46] D.G. Rickerby, N.H. Macmillan, The erosion of aluminum by solid particle impingement at oblique incidence, Wear 79 (Issue 2) (1982) 171–190, https://doi.org/10.1016/0043-1648(82)90166-1. ISSN 0043-1648.

[47] R.G. Bayer, P.A. Engel, E. Sacher, Impact wear phenomena in thin polymer films, Wear 32 (Issue 2) (1975) 181–194, https://doi.org/10.1016/0043-1648(75)90266-5. ISSN 0043-1648.

[48] S.L. Rice, Reciprocating impact wear testing apparatus, Wear 45 (Issue 1) (1977) 85–95, https://doi.org/10.1016/0043-1648(77)90104-1. ISSN 0043-1648.

[49] E.B. Iturbe, I.G. Greenfield, T.W. Chou, The wear mechanism obtained in copper by repetitive impacts, Wear 74 (Issue 1) (1981) 123–129, https://doi.org/10.1016/0043-1648(81)90198-8. ISSN 0043-1648.

[50] A. Ramalho, J.-P. Celis, Fretting laboratory tests: analysis of the mechanical response of test rigs, Tribol. Lett. 14 (No. 3) (2003), https://doi.org/10.1023/A:1022368414455.

[51] T. Slatter, Reducing Automotive Valve Recession Using Surface Treatments, PhD thesis, The University of Sheffield, U.K, 2010.

[52] R. Lewis, C. Tsoraki, J. Broughton, J.C. Cripps, S.A. Afodun, T. Slatter, V. Roubos, Abrasive and impact wear of stone used to manufacture axes in Neolithic Greece, Wear 271 (9) (2011) 2549–2560, https://doi.org/10.1016/j.wear.2010.12.074. ISSN 0043-1648.

[53] T. Slatter, R. Lewis, A.H. Jones, The influence of induction hardening on the impact wear resistance of compacted graphite iron (CGI), Wear 270 (3) (2011) 302–311, https://doi.org/10.1016/j.wear.2010.11.003. ISSN 0043-1648.

[54] T. Bruce, Analysis of the Premature Failure of Wind Turbine Gearbox Bearings, PhD thesis, The University of Sheffield, U.K, 2016, https://ethos.bl.uk/OrderDetails.do?uin=uk.bl.ethos.694145.